INTERNATIONAL JOURNAL FOR NUMERICAL METHODS IN FLUIDS
Int. J. Numer. Meth. Fluids 2007; **53**:201–227
Published online 19 June 2006 in Wiley InterScience (www.interscience.wiley.com). DOI: 10.1002/fld.1276

Pseudo-characteristic formulation and dynamic boundary conditions for computational aeroacoustics

Shang-Yi Lu[1,‡] and Pierre Sagaut[2,*,†]

[1]*Department of Mathematics, National University of Singapore, Singapore 117543, Singapore*
[2]*Laboratoire de Modélisation en Mécanique, Université Pierre et Marie Curie—Paris 6, 4, place Jussieu, case 162, 75252 Paris cedex 5, France*

SUMMARY

The present paper deals with the use of the pseudo-characteristic formulation of the Navier–Stokes and Euler equations recently introduced by Sesterhenn (*Comput. Fluid.* 2001; **30**:37–67) for the simulation of acoustic wave propagation. The emphasis is put on the formulation of an efficient method on structured curvilinear grids, along with the definition and implementation of efficient boundary conditions. The cases of inflow, outflow, rigid/compliant walls and walls with prescribed impedance are addressed. The proposed boundary conditions are assessed on generic cases. The pseudo-characteristic formulation enables a straightforward and optimal use of high-order upwind dispersion-relation-preserving schemes, yielding an efficient method. Copyright © 2006 John Wiley & Sons, Ltd.

Received 8 December 2005; Revised 11 April 2006; Accepted 11 April 2006

KEY WORDS: numerical scheme; Euler equation; computational aeroacoustics; boundary conditions

1. INTRODUCTION

Computational aeroacoustics (CAA), which consists in computing the generation of acoustic waves by an unsteady flow and the propagation of the acoustic waves through the fluid, is a rapidly growing field (see Reference [1] for an up-to-date presentation and Reference [2] for some recent examples). The two main reasons are the requirement to decrease the radiated sound level in many engineering processes and the growth of the available computing power.

The basic models for CAA are the Navier–Stokes equations and the Euler equations. The former is expected to yield an accurate description of both acoustic wave generation and propagation, while the later is mainly considered as a reliable model for wave propagation.

*Correspondence to: Pierre Sagaut, Laboratoire de Modélisation en Mécanique, Université Pierre et Marie Curie—Paris 6, 4, place Jussieu, case 162, 75252 Paris cedex 5, France.
†E-mail: pierre.sagaut@upmc.fr
‡E-mail: shangyi.lu@gmail.com

Therefore, one of the main CAA problem consists in finding an efficient method for solving these equations and modelling the physical problems of interest. This last requirement involves the capability of defining boundary conditions that accurately represent the true physical processes while minimizing the computational cost and preserving the numerical stability.

A huge amount of work has been devoted to the definition of numerical schemes for the Euler equations with good wave propagation properties. Among the most striking results, one can cite the family of the dispersion-relation-preserving schemes introduced by Tam and Webb [3, 4], the renewal of compact schemes [5–7] or the discontinuous Galerkin methods [8–11]. Several numerical schemes have been identified (see References [1, 12] for detailed surveys), which are accurate enough to simulate wave propagation in the linear regime over a few dozens of wavelengths. But it is important to note that the issue of the definition of a method which enables the proper handling of a wide set of boundary conditions, including complex ones such as time-domain impedance boundary conditions for liners or walls made of porous materials, is still an open issue.

The present paper deals with the use of the pseudo-characteristic formulation recently proposed by Sesterhenn [13] for the compressible Navier–Stokes equations on a curvilinear grid for CAA purpose. The emphasis is put on the discretization on structured curvilinear grids and the definition and implementation of efficient boundary conditions, including time-domain impedance boundary conditions. The boundary condition issue is known to be very important, since inaccurate boundary conditions can generate spurious waves which corrupt the results. A large amount of work has been devoted to this problem (see Reference [1] for a detailed review). A commonly agreed conclusion is that no fully general, satisfactory inflow/outflow boundary condition is available. The issue of representing solid boundary with prescribed, frequency-dependent impedance in the time domain is also an open problem, for which a very few solutions have been proposed.

The paper is organized as follows. Section 2 is devoted to the presentation of governing equations written in both Cartesian and curvilinear coordinates. Associated boundary conditions of practical interest for CAA purpose are presented in Section 3: inflow/outflow boundary conditions, sponge layer, rigid/compliant solid wall and solid wall with a prescribed impedance. Key elements of the numerical method are given in Section 4. Numerical accuracy of the method is investigated in Section 5. Numerical experiments dealing with the outflow boundary conditions are presented in Section 6, while the time-domain impedance boundary condition is assessed in Section 7. The accuracy of the proposed wall boundary condition versus the one obtained by the usual approximate solid wall boundary condition based on the extrapolation of some variables at the wall is checked in Section 8. Conclusions are given in Section 9.

2. PSEUDO-CHARACTERISTIC FORMULATION OF THE COMPRESSIBLE NAVIER–STOKES EQUATIONS

2.1. Governing equations in Cartesian coordinates

We first recall the main features of the pseudo-wave formulation introduced by Sesterhenn [13]. The 3D Navier–Stokes equations in terms of the pressure p, the velocity $\mathbf{u} = (u_1, u_2, u_3)$ and the

DOI: 10.1002/fld

entropy s are as follows, using the notation of repeated indices:

$$\begin{aligned} \frac{\partial \rho}{\partial t} + u_i \frac{\partial \rho}{\partial x_i} + \rho \frac{\partial u_i}{\partial x_i} &= 0 \\ \rho \left(\frac{\partial u_i}{\partial t} + u_j \frac{\partial u_i}{\partial x_j} \right) + \frac{\partial p}{\partial x_i} &= \frac{\partial \tau_{ij}}{\partial x_j} \\ \frac{\partial s}{\partial t} + u_i \frac{\partial s}{\partial x_i} &= \frac{1}{\rho T} \left(-\frac{\partial}{\partial x_i} \left(-\kappa \frac{\partial T}{\partial x_i} \right) + \Phi \right) \end{aligned} \tag{1}$$

where the viscous tensor is defined as

$$\tau_{ij} = 2\mu s_{ij} + \lambda \frac{\partial u_k}{\partial x_k} \delta_{ij}$$

and the tensor

$$s_{ij} = \frac{1}{2} \left(\frac{\partial u_i}{\partial x_j} + \frac{\partial u_j}{\partial x_i} \right)$$

with $3\lambda + 2\mu = 0$. We will refer to the thermally ideal gas throughout this paper:

$$p = \rho R T \tag{2}$$

The propagation of heat is given by Fourier's law:

$$q_j = -\kappa \frac{\partial T}{\partial x_j}$$

where T is the temperature (in Kelvins K) and κ the thermal conductivity. The constant κ can be expressed in terms of the dynamic viscosity μ by

$$\kappa = \frac{\mu C_p}{Pr}$$

where Pr is the Prandtl number, and C_p the specific heat at constant pressure, C_v the specific heat the constant volume, and the ratio of the specific heats is denoted by γ:

$$\gamma = \frac{C_p}{C_v}$$

Finally, viscous dissipation is denoted by

$$\Phi = \tau_{ij} s_{ij}$$

These equations, once discretized on a suitable grid, allows the direct numerical simulation of a compressible flow, and thus describe all non-stationary dynamics that results. They also allow us to describe the propagation of acoustic waves given that the grid resolution is adapted to the problem.

DOI: 10.1002/fld

As shown in Reference [13], fluxes can be rewritten in the following pseudo-characteristic form:

$$\begin{aligned}
\frac{\partial p}{\partial t} &= -\frac{\rho c}{2}((X^+ + X^-) + (Y^+ + Y^-) + (Z^+ + Z^-)) + \frac{p}{C_v}\left(\frac{\partial s}{\partial t} + X^s + Y^s + Z^s\right) \\
\frac{\partial u}{\partial t} &= -\left(\frac{1}{2}(X^+ - X^-) + Y^u + Z^u\right) + \frac{1}{\rho}\frac{\partial \tau_{1j}}{\partial x_j} \\
\frac{\partial v}{\partial t} &= -\left(X^v + \frac{1}{2}(Y^+ - Y^-) + Z^v\right) + \frac{1}{\rho}\frac{\partial \tau_{2j}}{\partial x_j} \\
\frac{\partial w}{\partial t} &= -\left(X^w + Y^w + \frac{1}{2}(Z^+ - Z^-)\right) + \frac{1}{\rho}\frac{\partial \tau_{3j}}{\partial x_j} \\
\frac{\partial s}{\partial t} &= -(X^s + Y^s + Z^s) + \frac{R}{p}\left(-\frac{\partial q_i}{\partial x_i} + \Phi\right)
\end{aligned} \tag{3}$$

where the following notations are used:

$$X^{\pm} = (u \pm c)\left(\frac{1}{\rho c}\frac{\partial p}{\partial x} \pm \frac{\partial u}{\partial x}\right) \tag{4}$$

$$X^v = u\frac{\partial v}{\partial x}, \quad X^w = u\frac{\partial w}{\partial x}, \quad X^s = u\frac{\partial s}{\partial x} \tag{5}$$

$$Y^{\pm} = (v \pm c)\left(\frac{1}{\rho c}\frac{\partial p}{\partial y} \pm \frac{\partial v}{\partial y}\right) \tag{6}$$

$$Y^u = v\frac{\partial u}{\partial y}, \quad Y^w = v\frac{\partial w}{\partial y}, \quad Y^s = v\frac{\partial s}{\partial y} \tag{7}$$

$$Z^{\pm} = (w \pm c)\left(\frac{1}{\rho c}\frac{\partial p}{\partial z} \pm \frac{\partial w}{\partial z}\right) \tag{8}$$

$$Z^u = w\frac{\partial u}{\partial z}, \quad Z^v = w\frac{\partial v}{\partial z}, \quad Z^s = w\frac{\partial s}{\partial z} \tag{9}$$

It is clearly seen that fluxes with $\pm$ superscripts (Equations (4), (6) and (8)) are related to acoustic waves (i.e. to disturbances which propagate at speed c with respect to the fluid), while the other ones correspond to fluctuations advected by the fluid. This new decomposition of the pressure, velocity and entropy fluxes enables a very simple and natural separation between acoustic and hydrodynamic disturbances. This feature will be of great help to define boundary conditions and stabilizing the numerical method.

2.2. Pseudo-characteristic formulation of the Navier–Stokes equations on a curvilinear grid

We now address the issue of the formulation of an efficient method on curvilinear grids. It is worth noting that most theoretical works deal with uniform grids (and most optimized schemes for wave

DOI: 10.1002/fld

propagation have been designed for uniform grid computation only) while a most practical CAA problems involve curvilinear grids. Therefore, the issue of finding a formulation of the governing equations which enables the control of the numerical error on curvilinear grids is of primary importance. This section addresses the extension of the above pseudo-wave formulation to the case of structured curvilinear grids. We follow here the original development by Sesterhenn [13].

Let us first introduce a coordinate mapping

$$\xi^j = \xi^j(x_i) \quad (i, j = 1, 2, 3)$$

and we will rewrite the Cartesian equations locally as waves which propagate normally to the surfaces $\xi^j = \text{constant}$.

We will note $\partial\xi^{(l)}/\partial x_i = \xi^l_{,i}$, and the contravariant velocity components as $u^l = \xi^l_{,i} u_i$.

Entropy transport will be decomposed into waves which propagate normally to the surfaces $\xi^l = \text{constant}$. Therefore, we define

$$\Theta^k_s = u^{(k)} \frac{\partial s}{\partial \eta^{(k)}} \tag{10}$$

where the upper index k indicates the contravariant transport direction and the lower index s identifies the entropy wave. Indices in brackets are not summed using the summation convention.

We define the following pseudo-wave terms:

$$\Theta^k_\pm = (u^{(k)} \pm c\sqrt{g^{(kk)}}) \left(\frac{1}{\rho c} \frac{\partial p}{\partial \xi^{(k)}} \pm \frac{\xi^{(k)}_{,i}}{\sqrt{g^{(kk)}}} \frac{\partial u_i}{\partial \xi^{(k)}} \right) \tag{11}$$

where $g^{lm} = \xi^l_{,i} \xi^m_{,i}$, and

$$\Theta^k_l = u^{(k)} \xi^l_{,i} \frac{\partial u_i}{\partial \xi^{(k)}} \tag{12}$$

which can also be expressed as follows:

$$\Theta^k_\pm = \left(u^{(k)} \pm c\sqrt{g^{(kk)}} \right) \left(\frac{2}{\gamma - 1} \frac{\partial c}{\partial \xi^{(k)}} - \frac{c}{\gamma R} \frac{\partial s}{\partial \xi^{(k)}} \pm \frac{\xi^{(k)}_{,i}}{\sqrt{g^{(kk)}}} \frac{\partial u_i}{\partial \xi^{(k)}} \right) \tag{13}$$

They are associated with disturbances propagating at speed $\left(u^{(k)} \pm c\sqrt{g^{(kk)}}\right)$.

The pseudo-characteristic formulation of the Navier–Stokes equations is as follows:

$$\begin{aligned}
\frac{\partial p}{\partial t} &= -\sum_{k=1}^{3} \frac{\rho c}{2} (\Theta^k_+ + \Theta^k_-) + \frac{p}{C_v} \left(\frac{\partial s}{\partial t} + \sum_{k=1}^{3} \Theta^k_s \right) \\
\frac{\partial u^1}{\partial t} &= -\frac{\sqrt{g^{11}}}{2} (\Theta^1_+ - \Theta^1_-) - \Theta^2_1 - \Theta^3_1 - \frac{1}{\rho} \left(\xi^1_{,l} \xi^2_{,l} \frac{\partial p}{\partial \xi^2} + \xi^1_{,l} \xi^3_{,l} \frac{\partial p}{\partial \xi^3} \right) + \frac{\xi^1_{,i} \xi^l_{,j}}{\rho} \frac{\partial \tau_{ij}}{\partial \xi^l} \\
\frac{\partial u^2}{\partial t} &= -\Theta^1_2 - \frac{\sqrt{g^{22}}}{2} (\Theta^2_+ - \Theta^2_-) - \Theta^3_2 - \frac{1}{\rho} \left(\xi^2_{,l} \xi^1_{,l} \frac{\partial p}{\partial \xi^1} + \xi^2_{,l} \xi^3_{,l} \frac{\partial p}{\partial \xi^3} \right) + \frac{\xi^2_{,i} \xi^l_{,j}}{\rho} \frac{\partial \tau_{ij}}{\partial \xi^l}
\end{aligned} \tag{14}$$

DOI: 10.1002/fld

$$\frac{\partial u^3}{\partial t} = -\Theta_3^1 - \Theta_3^2 - \frac{\sqrt{g^{33}}}{2}(\Theta_+^3 - \Theta_-^3) - \frac{1}{\rho}\left(\xi^3_{,l}\xi^1_{,l}\frac{\partial p}{\partial \xi^1} + \xi^3_{,l}\xi^2_{,l}\frac{\partial p}{\partial \xi^2}\right) + \frac{\xi^3_{,i}\xi^l_{,j}}{\rho}\frac{\partial \tau_{ij}}{\partial \xi^l}$$

$$\frac{\partial s}{\partial t} = -(\Theta_s^1 + \Theta_s^2 + \Theta_s^3) + \frac{1}{\rho T}\left(-\xi^l_{,i}\frac{\partial}{\partial \xi^l}\left(-\kappa\xi^l_{,i}\frac{\partial T}{\partial \xi^l}\right) + \Phi\right)$$

This new formulation is algebraically equivalent to (1). However, since we know the direction of the propagation of the different waves, we can use an upwind scheme to discretize each wave accordingly, which in turn guarantees the stability of the scheme and also welcomed properties of a DRP spatial scheme, which we will detailed later on.

3. DEFINITION OF EXACT CONSISTENT BOUNDARY CONDITIONS

A very interesting feature of the pseudo-characteristic formulation is that it enables a very accurate and simple implementation of the boundary conditions. The very reason why is that using this formulation the full Navier–Stokes equations are solved at boundary nodes, fluxes associated with incoming waves being prescribed in an adequate way to enforce the targeted physical effects. Since the full equations are solved at the boundary, and not replaced by simplified surrogate models, the pseudo-characteristic formulation is expected to have a greater potential than other formulations, which rely on the implementation of approximate boundary conditions.

3.1. Subsonic/supersonic outflow boundary conditions

The supersonic outflow boundary condition requires no special treatment: since the flow is supersonic, all advection speeds $u + c$, $u - c$ and u have the same sign, and all inviscid fluxes are computed at the boundary nodes using the high-order upwind scheme given by Equation (43). The full unmodified equations are therefore solved at the outflow plane.

The definition of subsonic non-reflecting boundary conditions is straightforward. Assuming that the outflow boundary is located at the node $i = Nx$, a non-reflecting boundary condition is obtained solving the Navier–Stokes equations while setting the incoming acoustic disturbance to zero (i.e. taking $X^- = 0$ in Equation (3)). The implementation of this condition is very easy, since it represents a minor modification in the method used at the interior nodes. It is important to note that this condition is exact, in the sense that all physical variables at the outflow plane are evaluated solving the full Navier–Stokes system. This non-reflecting boundary condition is easily extended to the case of curvilinear grids, setting $\Theta_-^1 = 0$ in (14).

A potential weakness of this very simple subsonic outflow condition is that the high-order upwind scheme is modified near the exit boundary, and it is well-known that a change in the numerical scheme can generate spurious reflected waves inside the computational domain (e.g. see Reference [14]). To minimize these spurious wave generation, a buffer layer technique can be very easily defined using the pseudo-characteristic formulation. It is here proposed to set $X^- = 0$ in the layer ranging from $i = Nx - 4$ to $i = Nx$, i.e. at all nodes at which the interior DRP scheme cannot be utilized. An alternative solution is to compute $X^- = 0$ with a first-order accurate upwind scheme in this region to damp incoming waves.

DOI: 10.1002/fld

3.2. Subsonic/supersonic inflow boundary conditions

The supersonic inflow condition is also immediately implemented, since it consists in prescribing the variation of all unknowns at the boundary nodes. This is equivalent to imposing $\partial p/\partial t$, $\partial u/\partial t$, $\partial v/\partial t$, $\partial w/\partial t$ and $\partial s/\partial t$ at each time step in (3), or to solve the Navier–Stokes equations. For a supersonic inlet, since the acoustic waves are not able to go back up the flow, we can prescribe the quantities $\partial p/\partial t$, $\partial u/\partial t$, $\partial v/\partial t$, and $\partial s/\partial t$ on the boundary for a 2D case.

These four quantities allow us to solve Equations (3). For an inlet on the left of the computational domain, we have

$$\begin{aligned}
X^s &= -Y^s + \frac{R}{p}\left(-\frac{\partial q_i}{\partial x_i} + \Phi\right) - \frac{\partial s}{\partial t} \\
X^v &= -\frac{1}{2}\left(Y^+ - Y^-\right) + \frac{1}{\rho}\frac{\partial \tau_{2j}}{\partial x_j} - \frac{\partial v}{\partial t} \\
X^+ &= -\left(\frac{Y^+ + Y^- + 2Y^u}{2}\right) + \frac{\gamma - 1}{\rho c}\left(-\frac{\partial q_i}{\partial x_i} + \Phi\right) + \frac{1}{\rho}\frac{\partial \tau_{1j}}{\partial x_j} - \frac{1}{\rho c}\frac{\partial p}{\partial t} - \frac{\partial u}{\partial t} \\
X^- &= \left(\frac{2Y^u - Y^+ - Y^-}{2}\right) + \frac{\gamma - 1}{\rho c}\left(-\frac{\partial q_i}{\partial x_i} + \Phi\right) - \frac{1}{\rho}\frac{\partial \tau_{1j}}{\partial x_j} - \frac{1}{\rho c}\frac{\partial p}{\partial t} + \frac{\partial u}{\partial t}
\end{aligned} \tag{15}$$

For curvilinear grids, we prescribe the same quantities as in the Cartesian case, which leads us to the following boundary conditions if we consider the Euler equations on the left boundary ($\xi^1 = 0$):

$$\begin{aligned}
\Theta_s^1 &= -\Theta_s^2 + \frac{1}{\rho T}\left(-\xi^l_{,i}\frac{\partial}{\partial \xi^l}\left(-\kappa \xi^l_{,i}\frac{\partial T}{\partial \xi^l}\right)\right) - \frac{\partial s}{\partial t} \\
\Theta_2^1 &= -\frac{\sqrt{g^{22}}}{2}(\Theta_+^2 - \Theta_-^2) - \frac{1}{\rho}\left(\xi^2_{,l}\xi^1_{,l}\frac{\partial p}{\partial \xi^1}\right) - \frac{\partial u^2}{\partial t} \\
\Theta_+^1 &= -\frac{1}{2}(\Theta_+^2 + \Theta_-^2) - \frac{1}{\sqrt{g^{11}}}\Pi_1^2 + \frac{\gamma - 1}{\rho c}\left(-\xi^l_{,i}\frac{\partial}{\partial \xi^l}\left(-\kappa \xi^l_{,i}\frac{\partial T}{\partial \xi^l}\right)\right) - \frac{1}{\rho c}\frac{\partial p}{\partial t} - \frac{1}{\sqrt{g^{11}}}\frac{\partial u^1}{\partial t} \\
\Theta_-^1 &= -\frac{1}{2}\left(\Theta_+^2 + \Theta_-^2\right) + \frac{1}{\sqrt{g^{11}}}\Pi_1^2 + \frac{\gamma - 1}{\rho c}\left(-\xi^l_{,i}\frac{\partial}{\partial \xi^l}\left(-\kappa \xi^l_{,i}\frac{\partial T}{\partial \xi^l}\right)\right) - \frac{1}{\rho c}\frac{\partial p}{\partial t} + \frac{1}{\sqrt{g^{11}}}\frac{\partial u^1}{\partial t}
\end{aligned} \tag{16}$$

where

$$\Pi_1^2 = \left(\Theta_1^2 + \frac{1}{\rho}\left(\xi^1_{,l}\xi^2_{,l}\frac{\partial p}{\partial \xi^2}\right)\right)$$

The pseudo-characteristic formulation also enables the definition of fully consistent exact inflow conditions in the subsonic case. Considering the case of a subsonic inflow condition at the boundary $i = 1$, one can see that the definition of such a condition is equivalent to prescribing X^+, X^s, X^v and X^w at this location at each time step. Since there are four unknown fluxes and five unknown physical variables, one recovers the well-known results that the time variation of all physical unknowns cannot be prescribed at the same time.

DOI: 10.1002/fld

A careful examination of system (3) shows that prescribing $\partial v/\partial t$ and $\partial w/\partial t$ is equivalent to prescribing values for X^v and X^w. To obtain a well-posed problem, one condition must be prescribed for each of these two velocity components. The three remaining physical variables (namely p, u and s) being coupled at the interface, they cannot be treated separately. A consistent inflow condition will therefore consists in finding values of $\partial p/\partial t$, $\partial s/\partial t$ and $\partial u/\partial t$ (or in an equivalent manner X^+ and X^s) at the inlet plane. A large number of combinations can be defined, depending on the prescribed quantities.

For example, if $\partial p/\partial t$ and $\partial s/\partial t$ are prescribed, then (3) yields

$$\begin{aligned} X^+ &= -((X^+ + X^-) + (Y^+ + Y^-)) + \frac{2}{\rho c}\left(\frac{p}{C_v}\left(\frac{\partial s}{\partial t} + X^s + Y^s\right) - \frac{\partial p}{\partial t}\right) \\ X^v &= -\left(\frac{\partial v}{\partial t} + \frac{1}{2}(Y^+ - Y^-)\right) + \frac{1}{\rho}\frac{\partial \tau_{2j}}{\partial x_j} \\ X^s &= -Y^s - \frac{\partial s}{\partial t} + \frac{R}{p}\left(-\frac{\partial q_i}{\partial x_i} + \Phi\right) \end{aligned} \tag{17}$$

If $\partial u/\partial t$ and $\partial s/\partial t$ are prescribed, then we obtain

$$\begin{aligned} X^+ &= X^- + 2Y^u + \frac{2}{\rho}\frac{\partial \tau_{1j}}{\partial x_j} - 2\frac{\partial u}{\partial t} \\ X^v &= -\left(\frac{\partial v}{\partial t} + \frac{1}{2}(Y^+ - Y^-)\right) + \frac{1}{\rho}\frac{\partial \tau_{2j}}{\partial x_j} \\ X^s &= -Y^s - \frac{\partial s}{\partial t} + \frac{R}{p}\left(-\frac{\partial q_i}{\partial x_i} + \Phi\right) \end{aligned} \tag{18}$$

It is important to note that these boundary conditions are exact, since they are directly derived from the Navier–Stokes equations without any assumptions. Therefore, they are consistent from a thermodynamic viewpoint.

3.3. Rigid/compliant isothermal wall

Now let us address now the modelling of an infinitely rigid or moving isothermal wall. In the 2D case, Equations (3) are of the following form:

$$\begin{aligned} \frac{\partial p}{\partial t} &= -\frac{\rho c}{2}((X^+ + X^-) + (Y^+ + Y^-)) + \frac{p}{C_v}\left(\frac{\partial s}{\partial t} + X^s + Y^s\right) \\ \frac{\partial u}{\partial t} &= -\left(\frac{1}{2}(X^+ - X^-) + Y^u\right) + \frac{1}{\rho}\frac{\partial \tau_{1j}}{\partial x_j} \\ \frac{\partial v}{\partial t} &= -\left(X^v + \frac{1}{2}(Y^+ - Y^-)\right) + \frac{1}{\rho}\frac{\partial \tau_{2j}}{\partial x_j} \\ \frac{\partial s}{\partial t} &= -(X^s + Y^s) + \frac{R}{p}\left(-\frac{\partial q_i}{\partial x_i} + \Phi\right) \end{aligned} \tag{19}$$

DOI: 10.1002/fld

Considering a solid wall located at the bottom of the computational domain, it is observed that the wall boundary condition is a particular case of the subsonic inflow conditions. The fluxes to be evaluated are Y^+, Y^u and Y^s, while prescribed quantities are the wall velocity and the isothermal constraint.

Some algebra yields the following relations for Y^u and Y^+:

$$Y^u = -\frac{\partial u}{\partial t} - \frac{1}{2}(X^+ - X^-) + \frac{1}{\rho}\frac{\partial \tau_{1j}}{\partial x_j} \tag{20}$$

$$Y^+ = 2\left(-\frac{\partial v}{\partial t} - X^v + \frac{1}{2}Y^- + \frac{1}{\rho}\frac{\partial \tau_{2j}}{\partial x_j}\right) \tag{21}$$

The wall-normal entropy flux Y^s is computed using the isothermal constraint in the following way:

$$\frac{\partial T}{\partial t} = 0 = \left.\frac{\partial T}{\partial p}\right|_s \frac{\partial p}{\partial t} + \left.\frac{\partial T}{\partial s}\right|_p \frac{\partial s}{\partial t} \tag{22}$$

Since $(\partial T/\partial p)|_s = [(\gamma - 1)/\gamma](T/p)$, and $(\partial T/\partial s)|_p = T/C_p$, we have

$$\frac{\partial p}{\partial t} = -\frac{\gamma p}{(\gamma - 1)C_p}\frac{\partial s}{\partial t} \tag{23}$$

Thus, together with (20) and (21), we have finally

$$Y^s = -X^s + \frac{R}{p}\left(-\frac{\rho c}{2}(X^+ + X^- + Y^+ + Y^-) + \gamma\left(-\frac{\partial q_i}{\partial x_i} + \Phi\right)\right) \tag{24}$$

The rigid wall boundary condition is recovered taking $\partial u/\partial t = \partial v/\partial t = 0$. The same system of equation can be used to model a porous boundary with a prescribed transpiration velocity. An important point is that, once again, the boundary condition is exact and fully consistent from a thermodynamic viewpoint.

On a curvilinear grid, the equations are

$$\begin{aligned}
\frac{\partial p}{\partial t} &= -\sum_{k=1}^{2}\frac{\rho c}{2}\left(\Theta_+^k + \Theta_-^k\right) + \frac{p}{C_v}\left(\frac{\partial s}{\partial t} + \sum_{k=1}^{2}\Theta_s^k\right)\\
\frac{\partial u^1}{\partial t} &= -\frac{\sqrt{g^{11}}}{2}(\Theta_+^1 - \Theta_-^1) - \Theta_1^2 - \frac{1}{\rho}\left(\xi^1_{,l}\xi^2_{,l}\frac{\partial p}{\partial \xi^2}\right) + \frac{\xi^1_{,i}\xi^l_{,j}}{\rho}\frac{\partial \tau_{ij}}{\partial \xi^l}\\
\frac{\partial u^2}{\partial t} &= -\Theta_2^1 - \frac{\sqrt{g^{22}}}{2}(\Theta_+^2 - \Theta_-^2) - \frac{1}{\rho}\left(\xi^2_{,l}\xi^1_{,l}\frac{\partial p}{\partial \xi^1}\right) + \frac{\xi^2_{,i}\xi^l_{,j}}{\rho}\frac{\partial \tau_{ij}}{\partial \xi^l}\\
\frac{\partial s}{\partial t} &= -(\Theta_s^1 + \Theta_s^2) + \frac{1}{\rho T}\left(-\xi^l_{,i}\frac{\partial}{\partial \xi^l}\left(-\kappa\xi^l_{,i}\frac{\partial T}{\partial \xi^l}\right) + \Phi\right)
\end{aligned} \tag{25}$$

DOI: 10.1002/fld

As before, we consider that the wall is situated on the lower boundary ($\xi^2 = 0$). Since the acoustic waves propagate normally to the surfaces $\xi^i = \text{constant}$, only the acoustic wave Θ^2_+ is unknown. Using $(25)_2$, we can obtain Θ^2_1:

$$\Theta^2_1 = -\frac{\partial u^1}{\partial t} - \frac{\sqrt{g^{11}}}{2}(\Theta^1_+ - \Theta^1_-) - \frac{1}{\rho}\left(\xi^1_{,l}\xi^2_{,l}\frac{\partial p}{\partial \xi^2}\right) + \frac{\xi^1_{,i}\xi^l_{,j}}{\rho}\frac{\partial \tau_{ij}}{\partial \xi^l}$$

On the other hand, $(25)_3$ will allow us to determine the unknown acoustic wave Θ^2_+:

$$\Theta^2_+ = \frac{2}{\sqrt{g^{22}}}\left(-\frac{\partial u^2}{\partial t} - \Theta^1_2 + \frac{\sqrt{g^{22}}}{2}\Theta^2_- - \frac{1}{\rho}\left(\xi^2_{,l}\xi^1_{,l}\frac{\partial p}{\partial \xi^1}\right) + \frac{\xi^2_{,i}\xi^l_{,j}}{\rho}\frac{\partial \tau_{ij}}{\partial \xi^l}\right)$$

To evaluate Θ^2_s we use as before the isothermal constraint which gives us

$$\frac{\partial p}{\partial t} = -\frac{\gamma p}{(\gamma - 1)C_p}\frac{\partial s}{\partial t}$$

and thus

$$\Theta^2_s = -\Theta^1_s + \frac{R}{p}\left(-\frac{\rho c}{2}(\Theta^1_+ + \Theta^1_- + \Theta^2_+ + \Theta^2_-) + \gamma\left(-\xi^l_{,i}\frac{\partial}{\partial \xi^l}\left(-\kappa \xi^l_{,i}\frac{\partial T}{\partial \xi^l}\right) + \Phi\right)\right)$$

3.4. Time-domain boundary condition for active walls with prescribed impedance

3.4.1. General. In this section, we will study the modelling of absorbent materials, which are used for the acoustic treatment of solid surfaces, for the simulation of propagation of acoustic waves in the temporal domain. The study will comprise absorbent walls of plane material with localized spatial reaction.

This modelling is necessary to represent some noise reduction devices, such as liners. Its objective is to represent, for incident acoustic waves, the properties of the material, and thus of the reflected wave. These properties are classically represented, in the ideal case of a plane wave of frequency ω in the absence of a flow, through the notion of impedance $\mathscr{Z}$, defined for a monochromatic wave to be the ratio between the acoustic pressure $\widehat{p}_a$, and the component of the acoustic velocity normal to the wall, $\widehat{v}_{a,n}$ at its surface:

$$\mathscr{Z} = \frac{\widehat{p}_a}{\widehat{v}_{a,n}} \tag{26}$$

where quantities with a *hat* are defined in the Fourier space. It is natural to normalize this quantity by the characteristic impedance of the medium ρc ($\approx 400\,\mathrm{kg\,m^{-2}\,s^{-1}}$ in air). This defines the reduced impedance, which is dimensionless:

$$Z = \frac{\mathscr{Z}}{\rho c} \tag{27}$$

A solid wall with prescribed impedance can be taken into account in a straightforward manner using the pseudo-characteristic formulation introducing the reflection coefficient $\widehat{W}$, which is the

DOI: 10.1002/fld

amplitude ratio of the incident acoustic wave and the reflected acoustic wave. If we consider that the acoustic waves propagate in the positive direction of y normal to the wall, we have:

$$\widehat{Y}^- = \widehat{W}\widehat{Y}^+ \tag{28}$$

In the following, for the sake of simplicity, we will consider the 1D inviscid case, where the acoustic wave propagates along the y axis in an inviscid fluid. The equations are thus

$$\begin{aligned} \frac{\partial p}{\partial t} &= -\frac{\rho c}{2}(Y^+ + Y^-) + \frac{p}{C_v}\left(X^s + \frac{\partial s}{\partial t}\right) \\ \frac{\partial v}{\partial t} &= 0 = -\left(\frac{1}{2}(Y^+ - Y^-)\right) \\ \frac{\partial s}{\partial t} &= -X^s \end{aligned} \tag{29}$$

By using $(29)_3$, $(29)_1$ becomes

$$\frac{\partial p}{\partial t} = -\frac{\rho c}{2}(Y^+ + Y^-) \tag{30}$$

Applying a temporal Fourier transform to this last equation and $(29)_2$, we can express the reduced impedance (by supposing that ρc is constant)

$$Z = \frac{\mathscr{Z}}{\rho c} = \frac{\widehat{Y}^+ + \widehat{Y}^-}{\widehat{Y}^+ - \widehat{Y}^-} \tag{31}$$

By using (28), we have

$$Z = \frac{1 + \widehat{W}}{1 - \widehat{W}} \tag{32}$$

which implies that

$$\widehat{W} = \frac{Z - 1}{Z + 1} \tag{33}$$

An interesting feature of this that the velocity at the wall (which is non-zero) will be directly computed solving the governing equations with the *ad hoc* value of the incoming acoustic flux. Therefore, it will be fully consistent with the pressure field. The condition of realizability is automatically satisfied since the image of the half-plane $\mathrm{Re}(Z) \geqslant 0$ via the transformation $(Z-1)/(Z+1)$ is the interior of the circle $|\widehat{W}| \leqslant 1$.

3.4.2. Implementation of a three-parameters impedance model. The impedance condition (28) is written in the frequency space, and must therefore be re-expressed in the time domain before it can be used in practical simulations. Since its direct translation in the time domain would introduce a convolution product with a infinite memory effect, it must be approximated using a nearly local (in time) model.

DOI: 10.1002/fld

In the following, we will use the three-parameters impedance model approximation proposed by Tam and Auriault [15], which is of the form

$$Z(\omega) = R_0 + i\left(\frac{X_{-1}}{\omega} + X_1\omega\right) \tag{34}$$

The condition of realizability is satisfied if $R_0 > 0$.

Considering Equation (28) and applying an inverse temporal Fourier transform, we have

$$Y^-(t) = -\int_{-\infty}^{\infty} W(t-\tau)Y^+(\tau)\,\mathrm{d}\tau \tag{35}$$

Fung and coworkers [16, 17] proposed to discretize this relation in the following manner:

$$Y^-(t) = \sum_{j=0}^{T/\Delta t} W(j\Delta t)Y^+(t - j\Delta t) \tag{36}$$

where T is the memory time of the kernel of convolution W. For model (34), we have

$$W(t) = H(t)\tilde{W}(t) - \delta(t) \tag{37}$$

where H is the Heaviside function, and δ the Dirac delta, and

$$\tilde{W}(t) = \left(\frac{2}{X_1}\right)\left(\cos(\beta t) - \frac{\alpha}{\beta}\sin(\beta t)\right)\exp(-\alpha t) \tag{38}$$

with

$$\alpha = \frac{1+R_0}{2X_1}, \quad \beta = \sqrt{\omega_0^2 - \alpha^2}, \quad \omega_0 = \sqrt{\frac{X_{-1}}{X_1}} \tag{39}$$

In the presence of a flow with an average Mach number M_0, and a plane wall which is normal to the y axis and a 2D problem, we will use the discrete form suggested by Fung *et al*. [16, 17]:

$$Y^-(t) = \Delta t S_I(t) + 2M_0 S_{II}(t) - \left(\frac{\Delta t}{X_1} + 1\right)Y^+(t) \tag{40}$$

where $S_I(t)$ and $S_{II}(t)$ can be calculated using a recursive form:

$$\begin{aligned} S_I(t) &= 2\cos(\beta t)\exp(-\alpha\Delta t)S_I(t-\Delta t) - \exp(-2\alpha\Delta t)S_I(t-2\Delta t) \\ &\quad + \frac{2}{X_1}\left[Y^+(t) - \left(\cos(\beta\Delta t) + \frac{\alpha}{\beta}\sin(\beta\Delta t)\right)\exp(-\alpha\Delta t)Y^+(t-\Delta t)\right] \\ S_{II}(t) &= 2\cos(\beta t)\exp(-\alpha\Delta t)S_{II}(t-\Delta t) - \exp(-2\alpha\Delta t)S_{II}(t-2\Delta t) \\ &\quad + \frac{1}{X_1\beta}\sin(\beta\Delta t)\exp(-\alpha\Delta t)\frac{\partial}{\partial x}p(t-\Delta t) \end{aligned}$$

DOI: 10.1002/fld

3.4.3. Active wall boundary condition. Further, assuming that the tangential velocity component u is zero (this makes sense since the transpiration velocity is expected to be much larger than the tangential velocity at the wall), i.e. setting $\partial u/\partial t = 0$, one obtains the following time-domain boundary condition for active walls with prescribed impedance:

$$\begin{aligned} Y^u &= -\tfrac{1}{2}(X^+ - X^-) \\ Y^-(t) &= \Delta t S_I(t) + 2M_0 S_{II}(t) - \left(\frac{\Delta t}{X_1} + 1\right) Y^+(t) \\ Y^s &= -X^s + \frac{R}{p}\left(-\frac{\rho c}{2}(X^+ + X^- + Y^+ + Y^-) + \gamma\left(-\frac{\partial q_i}{\partial x_i} + \Phi\right)\right) \end{aligned} \tag{41}$$

The infinitely rigid impermeable wall condition is recovered taking $Z = +\infty$, and thus (33) implies that,

$$\widehat{W} = 1$$

By choosing

$$\frac{\partial v}{\partial t} = 0$$

for a 2D flow, one recovers the usual perfectly rigid wall condition from $(29)_2$

$$Y^- = Y^+$$

4. NUMERICAL METHOD

This new decomposition of the pressure, velocity and entropy fluxes enables a very simple and natural use of upwind schemes to enforce numerical stability while minimizing the numerical dissipation.

In the present work, all inviscid fluxes are written in a quasi-linear form and appear under the generic form $(u(\partial\phi/\partial x))$, where u is the advecting velocity and ϕ the advected quantity. To enforce both numerical stability and accuracy for wave propagation problems, it is chosen here to use high-order upwind dispersion-relation-preserving schemes for all fluxes.

At interior nodes (i.e. for grid point with index $5 \leqslant i \leqslant Nx - 2$, where Nx is the index of the last grid point) the following fourth-order accurate upwind-biased DRP scheme [18] is used:

$$\left(u\frac{\partial\phi}{\partial x}\right)_i = u_i \frac{1}{\Delta x} \sum_{k=-4,\,2} a_k \phi_{i+k} \tag{42}$$

with

$$a_{-4} = 0.0161404967151, \quad a_{-3} = -0.122821279020, \quad a_{-2} = 0.455332277706$$

$$a_{-1} = -1.2492595882615, \quad a_0 = 0.5018904380193, \quad a_1 = 0.4399321927296$$

$$a_2 = -0.04121453788895$$

DOI: 10.1002/fld

where it was assumed that the convection speed u is positive. The above DRP scheme is modified as follows near the computational domain boundaries:

- at $i = Nx$, a sixth-order one-sided upwind scheme is utilized:

$$\left(u\frac{\partial\phi}{\partial x}\right)_i = u_i \frac{1}{\Delta x} \sum_{k=-6,\,0} a_k \phi_{i+k}$$

$$a_{-6} = 1/60, \quad a_{-5} = -6/5, \quad a_{-4} = 15/4, \quad a_{-3} = 20/3, \quad a_{-2} = 15/2 \qquad (43)$$

$$a_{-1} = -6, \quad a_0 = 49/20$$

- at $i = Nx - 1$, the following upwind-biased DRP scheme proposed in Reference [18] is implemented:

$$\left(u\frac{\partial\phi}{\partial x}\right)_i = u_i \frac{1}{\Delta x} \sum_{k=-5,\,1} a_k \phi_{i+k}$$

$$a_{-5} = -0.0306489732244242, \quad a_{-4} = 0.202225858313369$$

$$a_{-3} = -0.634728026533812, \quad a_{-2} = 1.29629965415671 \qquad (44)$$

$$a_{-1} = -2.14305478803459, \quad a_0 = 1.10888726751399$$

$$a_1 = 0.201019007808754$$

- at $i = 4$, a fifth-order upwind-biased scheme is used:

$$\left(u\frac{\partial\phi}{\partial x}\right)_i = u_i \frac{1}{\Delta x} \sum_{k=-3,\,2} a_k \phi_{i+k} \qquad (45)$$

$$a_{-3} = -1/30, \quad a_{-2} = 1/4, \quad a_{-1} = -1, \quad a_0 = 1/3 \quad a_1 = 1/2, \quad a_2 = -1/20$$

- at $i = 3$, it is replaced by the following third-order upwind scheme:

$$\left(u\frac{\partial\phi}{\partial x}\right)_i = u_i \frac{1}{\Delta x} \sum_{k=-2,\,1} a_k \phi_{i+k} \qquad (46)$$

$$a_{-2} = 1/6, \quad a_{-1} = -1, \quad a_0 = 1/2, \quad a_1 = 1/3$$

- at $i = 2$, the first-order upwind scheme is used:

$$\left(u\frac{\partial\phi}{\partial x}\right)_i = u_i \frac{1}{\Delta x} \sum_{k=-1,\,0} a_k \phi_{i+k} \qquad (47)$$

$$a_{-1} = -1, \quad a_0 = 1$$

DOI: 10.1002/fld

- at $i = 1$, the following downwind scheme is used:

$$\left(u\frac{\partial\phi}{\partial x}\right)_i = u_i \frac{1}{\Delta x}\sum_{k=0,\,2} a_k \phi_{i+k}$$
$$a_0 = -3/5, \quad a_1 = 4/5, \quad a_2 = -1/5 \tag{48}$$

The time integration is performed using the third-order TVD Runge–Kutta scheme proposed by Shu and Osher [19]:

$$\begin{aligned} u^{n,1} &= u^n + \Delta t\left(\frac{\partial u^n}{\partial t}\right) \\ u^{n,2} &= \frac{1}{4}\left(3u^n + u^{n,1} + \Delta t\left(\frac{\partial u^{n,1}}{\partial t}\right)\right) \\ u^{n+1} &= \frac{1}{3}\left(u^n + 2u^{n,2} + 2\Delta t\left(\frac{\partial u^{n,2}}{\partial t}\right)\right) \end{aligned} \tag{49}$$

5. ASSESSMENT OF THE NUMERICAL METHOD ACCURACY

We consider the advection of a 2D entropy spot by a subsonic uniform flow, which is described in more details in Section 6.4. Here we take the final time to be $t_f = 3.75 \times 10^{-3}$, such that the density perturbation is still in the computational domain, and more importantly, has not reached the boundary. In this case, we are able to compute the analytic solution ρ_a and compare it with the numerical solution ρ_n without any influence of the outflow boundary condition. Hence, we consider the L^1 and L^2 norms of $\text{err} = \|\rho_n - \rho_a\|$ at t_f. Results displayed in Figure 1 show that the method exhibits the theoretical fourth-order of accuracy on uniform grids, while it is third-order accurate on curvilinear grids.

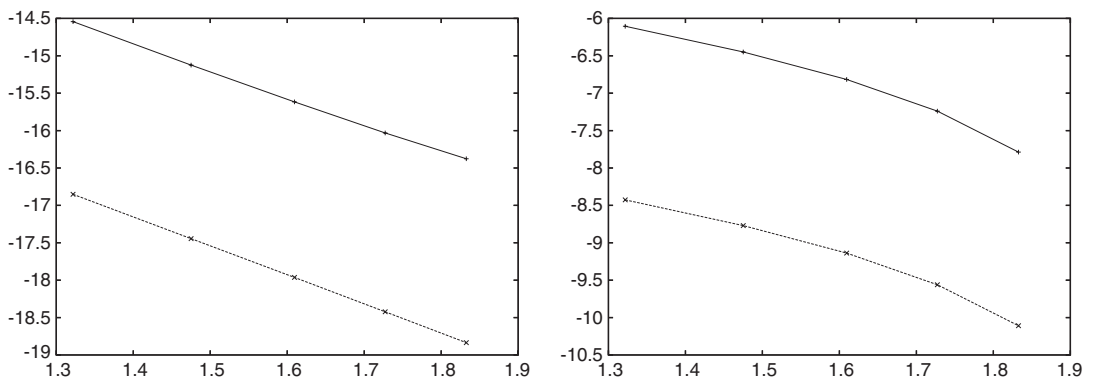

Figure 1. $\log\|\rho_n - \rho_a\|_{L^1}$ (+) and $\log\|\rho_n - \rho_a\|_{L^2}$ (×) expressed as a function of $\log\Delta x$ for a uniform (left) and curvilinear (right) simulation of a 2D entropy spot.

DOI: 10.1002/fld

6. OUTFLOW BOUNDARY CONDITIONS ASSESSMENT

This section is devoted to the presentation of numerical results dealing with the accuracy of the outflow boundary conditions. The accuracy is assessed for each type of Kovasznay mode [20] (namely: entropy mode, acoustic mode and vorticity mode). The efficiency on curvilinear grids is also investigated.

6.1. 1D acoustic wave

We will first present the results obtained when considering an acoustic disturbance in a fluid at rest. The domain is defined as $[-40, 0]$ and exit boundary conditions are applied on both extremities of the computational domain. The mesh is uniform with $\Delta x = 0.2$. The initial perturbation is defined as

$$\rho(x, t=0) = \varepsilon \, \mathrm{e}^{-\alpha x^2}, \quad \alpha = \frac{\log 2}{b^2}$$

$$p(x, t=0) = c_0^2 \rho(x, t=0)$$

$$u(x, t=0) = 0$$

with $b = 3$ and $\varepsilon = 0.01$. Results obtained with CFL $= 0.2$ are illustrated in Figure 2.

The time history of the norm L^1 of the quantity E_t/E_0 is displayed in Figure 3, where E_t and E_0 are the total energy (sum of the internal energy and the kinetic energy) of the perturbation at time t and the initial time, respectively. It is observed that at large time the residual value, which corresponds to the total energy of the numerical error, is of the order of 10^{-8}, showing very good properties of the present outflow boundary condition. This level of error corresponds to the maximum accuracy that can be obtained on the computer utilized during this work. A careful examination also reveals the existence of a transient phase associated to the propagation of a reflected spurious acoustic wave whose energy is 5×10^{-6} times lower than the initial wave.

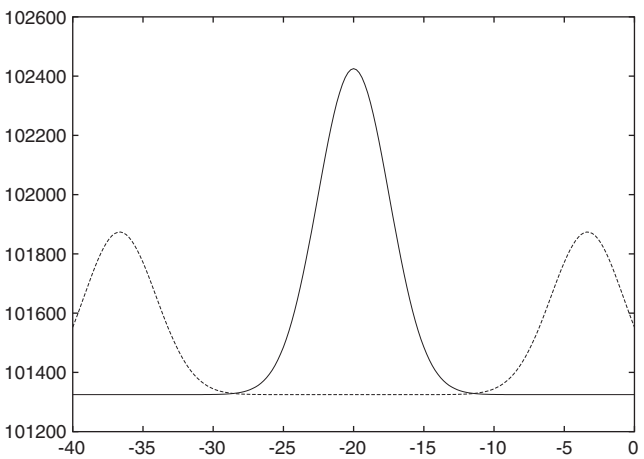

Figure 2. Instantaneous pressure (in Pa) at time $t = 0$ (—) and $t = 0.1$ (- -).

DOI: 10.1002/fld

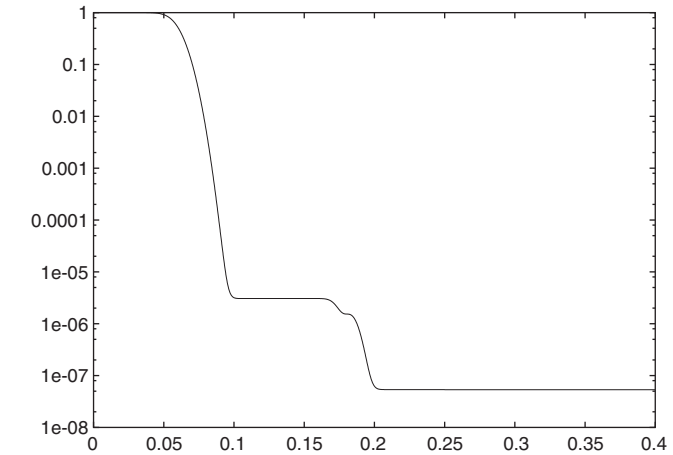

Figure 3. Time history of the norm L^1 of E_t/E_0 with CFL $= 0.2$.

Table I. Final value of the energy of the residual perturbation versus the CFL number.

CFL	$\|E_{0.4}/E_0\|_{L^1}$
0.1	5.0609×10^{-8}
0.2	5.3303×10^{-8}
0.5	9.8096×10^{-8}

The sensitivity of the outflow condition with respect to the value of the CFL number is now investigated repeating the simulation, and compared the numerical values obtained for the quantity $\|E_t/E_0\|_{L^1}$. The final time is $t = 0.4$. The results are summarized in Table I. It is observed that the error exhibits a slight sensitivity.

The dependence upon the sharpness of the propagated profile is now investigated by varying the value of b. The forms of the initial perturbations and the corresponding time histories of the fluctuating total energy are displayed in Figure 4. The final residual is seen to increase as b decreases, i.e. as the number of grid points located within the acoustic wave is reduced. The final values of the residual are given in Table II.

6.1.1. Acoustic sponge zone. As mentioned above, the simulation experiences a non-negligible loss of precision near the boundary since a high-order upwind scheme cannot be utilized for the grid points near the boundary in each direction. A consequence is the existence of a reflected spurious wave, as observed in the previous test case. Thus, we introduce a sponge zone, that is to say a layer in which the growth of spurious reflected waves will be prevented. The pseudo-characteristic formulation makes it possible to define and to implement very easily such a sponge layer. In the present simulation, we impose that $X^+ = 0$ for the first 5 grid points and $X^- = 0$ for the last 5 grid points in the positive direction of the x axis.

DOI: 10.1002/fld

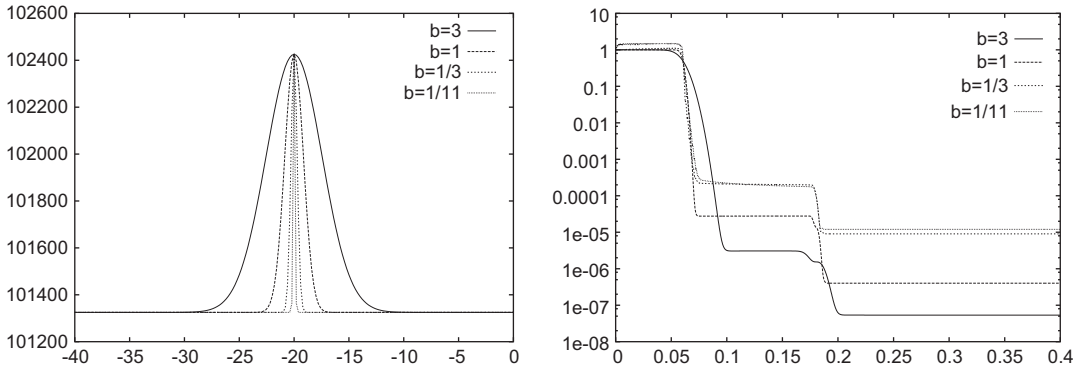

Figure 4. Initial pressure profile (expressed in Pa) with $b=3$, $b=1$, $b=\frac{1}{3}$, $b=\frac{1}{11}$ (left), and corresponding histories of L^1 norm of E_t/E_0 (right).

Table II. Final value of the energy of the residual perturbation versus b.

b	$\|E_{0.4}/E_0\|_{L^1}$
3	5.3303×10^{-8}
1	4.6160×10^{-7}
$\frac{1}{3}$	9.0317×10^{-6}
$\frac{1}{11}$	1.2010×10^{-5}

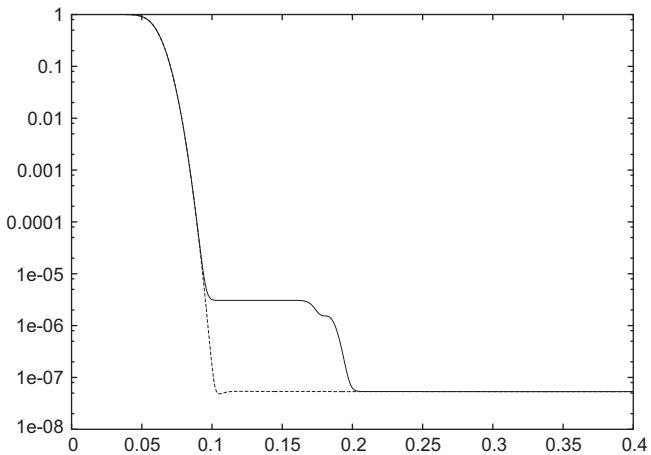

Figure 5. Time history of L^1 norm of E_t/E_0 without (—) and with (- -) a sponge zone.

The simulation is carried out with CFL $= 0.2$ and $b = 3$. Time history of the fluctuating energy is displayed in Figure 5. We observe that the presence of a sponge zone absorbs almost perfectly the reflected numerical waves.

DOI: 10.1002/fld

6.2. 2D acoustic wave

As in the 1D case, we study the evolution of an initial 2D acoustic pulse. The computational domain is $[-40, 0]^2$ and exit boundary conditions are applied on all boundaries of the computational domain. The initial disturbance is defined as

$$\rho(x, y, t=0) = \varepsilon \, \mathrm{e}^{-\alpha(x^2+y^2)}$$

$$p(x, y, t=0) = c_0^2 \rho(x, y, t=0)$$

$$u(x, y, t=0) = 0$$

$$v(x, y, t=0) = 0$$

with $\varepsilon = 0.01$ and $b = 3$ and CFL $= 0.2$. The time final for the simulations is taken at $t = 0.5$. The instantaneous pressure field at different times is displayed in Figure 6. The norm L^1 of the normalized residual energy E_t/E_0 is of the order of 10^{-3}, and it is observed that the error concentrates in regions located near boundaries where the numerical accuracy is modified.

The same numerical test have been carried out on a curvilinear grid in order to investigate the accuracy of the method on non-orthogonal grids. The parameters are as in the Cartesian case: CFL $= 0.2$, $b = 3$ and $\varepsilon = 0.01$ with $t = 0.5$ being the final time. The curvilinear grid (which is

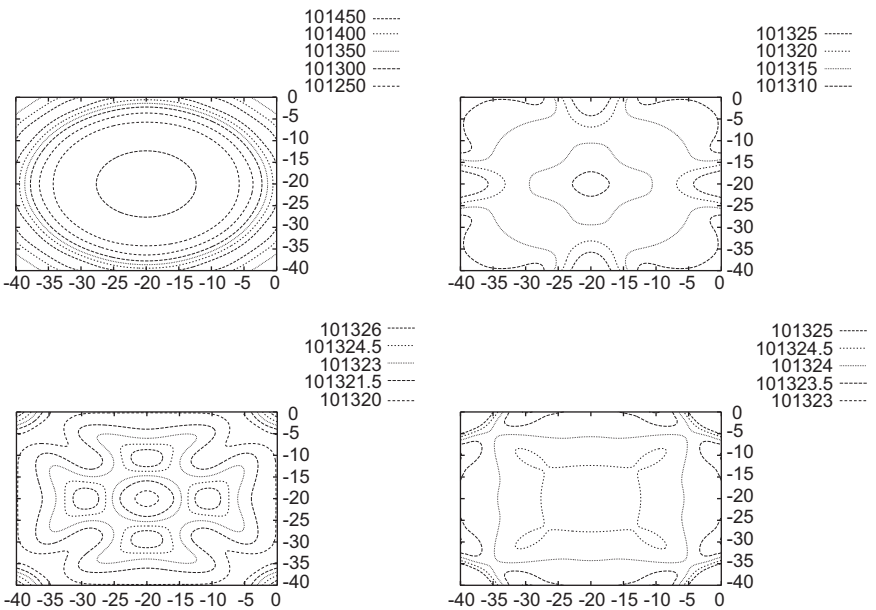

Figure 6. Contours of the acoustic wave from $500\Delta t$ to $2000\Delta t$ with interval $500\Delta t$ (from left to right and top to bottom).

DOI: 10.1002/fld

Table III. Residual fluctuating energy on uniform and curvilinear grids for the two forms of the acoustic fluxes.

Grid	E_t/E_0 using (11)	E_t/E_0 using (13)
Uniform grid	1.4086×10^{-3}	1.2472×10^{-3}
Curvilinear grid	1.65×10^{-3}	1.5315×10^{-3}

a perturbation of a Cartesian grid by a sine function), is defined analytically by

$$\xi^1 = x + \frac{\Delta x}{4} \sin y$$

$$\xi^2 = y + \frac{\Delta y}{4} \sin x$$

To discretize the metrics,

- at $i = Nx$, a first-order scheme is used:

$$\left(\frac{\partial \xi^j}{\partial x}\right)_i = \frac{\xi_i^j - \xi_{i-1}^j}{\Delta x} \tag{50}$$

- at $2 \leqslant i \leqslant Nx - 1$, we use the following second-order scheme:

$$\left(\frac{\partial \xi^j}{\partial x}\right)_i = \frac{\xi_{i+1}^j - \xi_{i-1}^j}{2\Delta x} \tag{51}$$

- at $i = 1$, a first-order scheme is used:

$$\left(\frac{\partial \xi^j}{\partial x}\right)_i = \frac{\xi_{i+1}^j - \xi_i^j}{\Delta x} \tag{52}$$

Time histories of the L^1 norm of E_t/E_0 are summarized in Table III.

The method is seen to be as accurate on curvilinear grids as on Cartesian grids, the magnitude of the residual disturbance being the same. In addition, formulation (13) gives slightly better results, and therefore must be preferred.

6.3. The 1D entropy wave

We now present results obtained when considering an initial Gaussian density perturbation in a uniform subsonic flow. The Mach number is taken equal to 0.5. The computational domain is the same as in the case of the 1D acoustic wave. Inflow and outflow boundary conditions are applied, respectively, on the left and right of the computational domain. The mesh is uniform with

DOI: 10.1002/fld

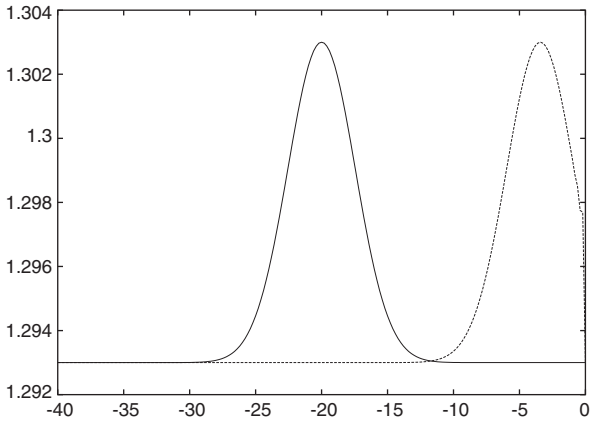

Figure 7. Instantaneous density profile at time $t = 0$ (—) and $t = 0.05$ (- -).

$\Delta x = 0.2$. The initial perturbation is defined as

$$\rho(x, t = 0) = \varepsilon \, \mathrm{e}^{-\alpha x^2}$$

$$p(x, t = 0) = 0$$

$$u(x, t = 0) = 0$$

with CFL $= 0.2$, $b = 3$, $\varepsilon = 0.01$ and time final $t = 0.5$. The evolution of the density field is illustrated in Figure 7. The maximum residual amplitude of the density perturbation is of the order of 10^{-6} of the initial perturbation, and thus showing good properties of the present method.

6.4. 2D entropy spot

As in the 2D case for the acoustic wave, the computational domain is $[-40, 0]^2$. Subsonic inlet and subsonic outlet boundary conditions are applied, respectively, on the left and right of the computational domain. The mesh is uniform with $\Delta x = \Delta y = 0.2$. The flow is uniform and subsonic with a Mach number which is equal to 0.5. The initial perturbation is defined as follows:

$$\rho(x, t = 0) = \varepsilon \, \mathrm{e}^{-\alpha(x^2 + y^2)}$$

$$p(x, t = 0) = 0$$

$$u_r(x, t = 0) = 0$$

$$u_\theta(x, t = 0) = 0$$

The parameters chosen are CFL $= 0.1$, $b = 3$ and $\varepsilon = 0.01$. Instantaneous plots of the density perturbation at time $t = 0$ and $t = 0.2$ are given in Figure 8.

As in the case of the 2D acoustic wave, we carry out the same test on a curvilinear grid, with the following parameters: CFL $= 0.2$, $b = 3$ and $\varepsilon = 0.01$ with $t_{\text{final}} = 0.5$. The residual values of

DOI: 10.1002/fld

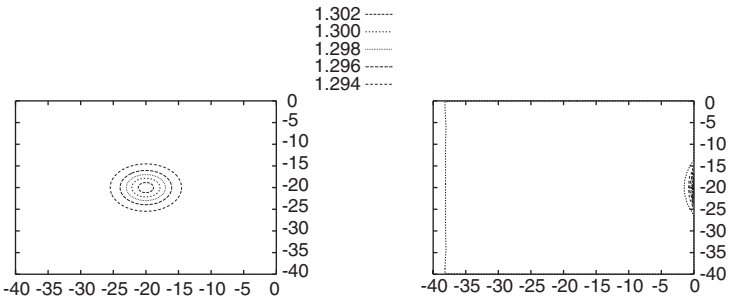

Figure 8. Contours of instantaneous density field at time $t = 0$ (left) and $t = 0.1$ (right).

Table IV. Norm of the residual error on density.

Grid	$\|\rho_t/\rho_0\|_{L^1}$
Uniform grid	6.6426×10^{-5}
Curvilinear grid	6.6424×10^{-5}

$\|\rho_t/\rho_0\|_{L^1}$ are presented below in Table IV. The residual spurious fluctuation is observed to be negligible, and the accuracy is preserved on the curvilinear grid.

6.5. *Vortex advection by a uniform flow*

At $t = 0$, we introduce at the centre of the computational domain, a 2D vortex with the following initial conditions:

$$u_x(x, y) = u_0 + a_0 y \exp[-\ln 2(x^2 + y^2)]$$

$$u_y(x, y) = -a_0 x \exp[-\ln 2(x^2 + y^2)]$$

with $a_0 = 10\,\mathrm{ms}^{-1}$. The flow is uniform with the Mach number equal to 3, with the computational domain being $[-10, 10]^2$ and a uniform mesh $\Delta x = \Delta y = 0.1$.

For the boundary conditions, we use the Equations (15). The evolution of the pressure field is presented in Figure 9.

The time history of the norms L^1 of the vorticity and the pressure perturbation are presented in Figure 10. To take into account the generation of spurious reflected waves inside the computational domain, we present in addition, the time history of the norms L^1 of the vorticity and the pressure perturbation, outside the five-cell-wide region in which the numerical accuracy is changed in front of the outlet boundary (i.e. $Nx - 4 \leqslant i \leqslant Nx$). It is observed that 99% of the L^1 norm of the error originates in this region, and that very satisfactory results are obtained outside this outlet layer.

DOI: 10.1002/fld

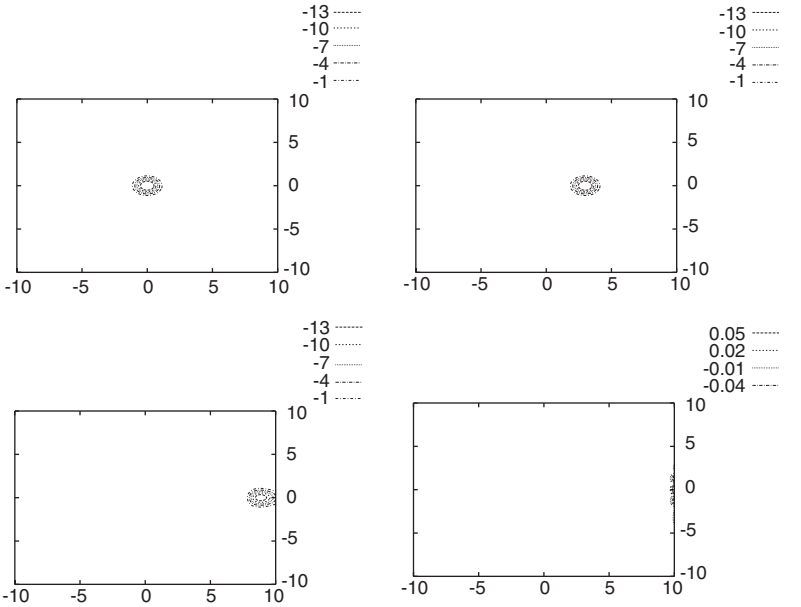

Figure 9. Contours of the vortex pressure field from $t = 0$ to $500\Delta t$ (from left to right and top to bottom).

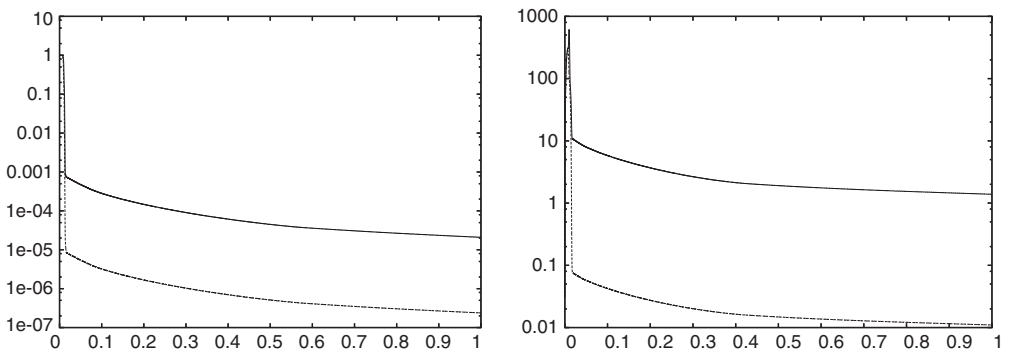

Figure 10. History of L^1 norm of the vorticity (right) and the pressure (left) perturbation: (–) full computational domain, (- -) outside outlet layer.

7. ACTIVE WALL BOUNDARY CONDITION ASSESSMENT

We now check the accuracy of the time-domain impedance condition defined in Section 3.4 by considering the canonical case of a monochromatic plane acoustic wave that impinges on a wall with a prescribed impedance. The experimental case of the 6.7% perforate treatment panel studied

DOI: 10.1002/fld

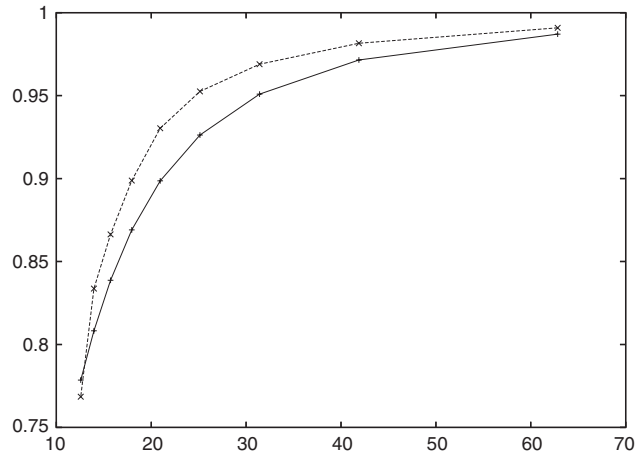

Figure 11. Numerical (×) and theoretical (+) values for the amplitude of the reflected wave expressed as a function of the PPW factor, for varying Ω.

by Motsinger and Kraft [21] is used here, since experimental values of R and X are available. Following Tam and Auriault [15], the parameters of the impedance model (34) are taken as follows: $R_0 = 0.2$, $X_{-1} = 13\,480$, and $X_1 = 0.0000739$.

The initial pressure perturbation is defined as follows:

$$p(x, y, t = 0) = p_0 + 2\cos(\Omega y/c)$$

The efficiency of the method is checked by comparing the computed amplitude of the reflected wave for different values of Ω with its theoretical value. The computational domain is $[-0.02, 0]$ and the same uniform mesh with $\Delta y = 10^{-4}$ is utilized for all simulations. The CFL number (based on the speed of sound) is taken equal to 0.5. It is worth noting that varying Ω is equivalent to changing the wavelength of the incident wave. Since both the grid and CFL number are kept constant, the number of grid point per wavelength (PPW) varies with Ω. For a frequency Ω of 1 kHz, we use 62.8 grid points to discretize each wavelength. At the highest considered frequency, which is equal to 5 kHz, the PPW factor is equal to 12.6, ensuring that the wave propagation phenomena will be correctly captured outside the wall region. The computed and exact amplitudes are displayed in Figure 11, and the relative error is plotted in Figure 12. A satisfactory agreement is recovered since the relative error is within 5% in all cases, showing the efficiency of the proposed time-domain impedance condition.

In order to check the convergence of the boundary condition with respect to the PPW factor, a second set of simulations was carried out with fixed Ω and CFL but varying grid resolution. The relative error committed on the amplitude of the reflected wave versus the PPW for $\Omega = 1$ kHz is plotted in Figure 13. It is seen that the maximum relative error level can be significant if the PPW factor is not high enough. The error induced by the time-impedance model is much higher than the one introduced by the DRP scheme used to compute the fluxes, and the computational grid must therefore be designed to enforce an acceptable error level at the active wall boundary.

DOI: 10.1002/fld

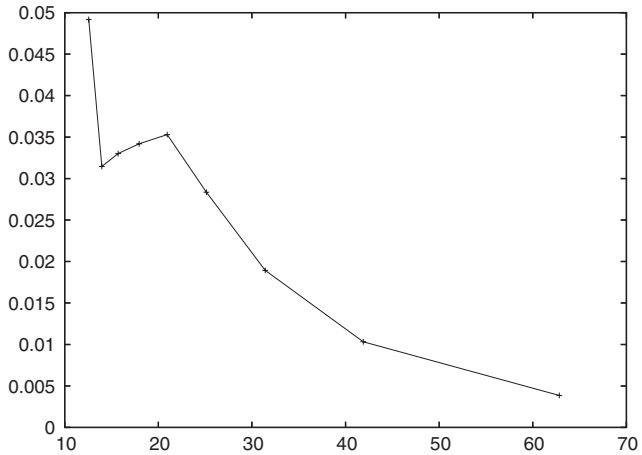

Figure 12. Relative numerical error in the evaluation of the amplitude of the reflected wave versus the PPW factor, for varying Ω.

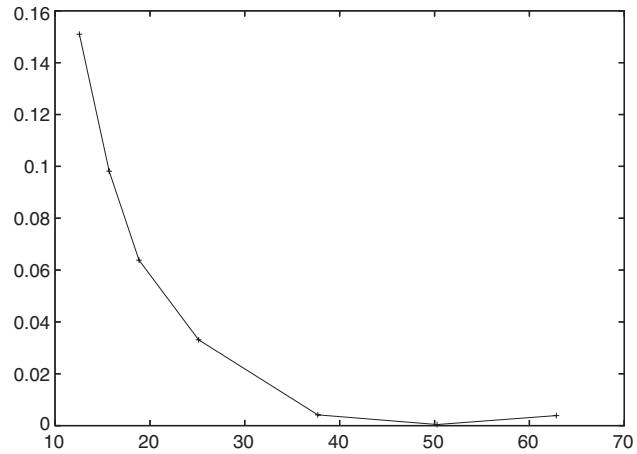

Figure 13. Numerical error in the evaluation of the amplitude, with $\Omega = 1$ kHz.

8. INFINITELY RIGID IMPERMEABLE WALL BOUNDARY CONDITION ASSESSMENT

We now compare the accuracy of the infinitely rigid impermeable wall condition defined in Section 3.4 with the following first-order approximations:

$$u_{i,1} = 0 \qquad \forall\ 1 \leqslant i \leqslant Nx$$

$$v_{i,1} = 0 \qquad \forall\ 1 \leqslant i \leqslant Nx$$

$$p_{i,1} = p_{i,2} \qquad \forall\ 1 \leqslant i \leqslant Nx$$

$$s_{i,1} = s_{i,2} \qquad \forall\ 1 \leqslant i \leqslant Nx$$

DOI: 10.1002/fld

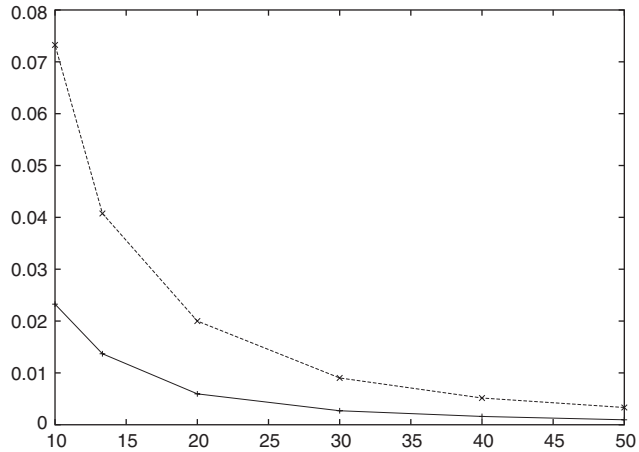

Figure 14. Relative numerical error using pseudo-characteristic formulation (+) versus relative numerical error using a first-order approximation (×) for the amplitude of the reflected wave expressed as a function of the PPW factor, for varying Ω.

The initial pressure perturbation is defined as follows:

$$p(x, y, t = 0) = p_0 + 2\cos(\Omega y/c)$$

We note that the boundary conditions obtained using Sesterhenn's formulation are exact. By imposing $Y^+ = Y^-$ at the boundary, the amplitude of the incident and reflected waves are forced to be identical. Hence, we check the efficiency of the method by comparing the computed amplitude of the reflected wave over a wavelength near the exit of the computational domain. The computational domain is $[-2, 0]$ and the same uniform mesh with $\Delta y = 10^{-2}$ is utilized for all simulations. The CFL number is taken equal to 0.2. Since both the grid and CFL number are kept constant, the number of grid point per wavelength (PPW) varies with Ω. We consider the PPW factor varying between 10 and 50. The relative numerical error for both Sesterhenn's formulation and the first-order approximation used is plotted in Figure 14. It is clear that Sesterhenn's boundary conditions gives better results.

9. CONCLUSION

A numerical method well-suited for CAA purposes was presented and assessed. It relies on the pseudo-characteristic formulation of the Navier–Stokes equations recently proposed by Sesterhenn. A very interesting feature of this formulation is that it provides an explicit splitting of the fluxes between hydrodynamic, entropy and acoustic disturbances. It has been shown that the accuracy of the method on curvilinear grid can be improved using a specific decomposition of the acoustic fluxes. A wide set of boundary conditions has been proposed and assessed, including time-domain impedance boundary condition, which is proved to be efficient. An important feature of the pseudo-characteristic formulation is that it enables the definition of thermodynamically consistent boundary conditions.

DOI: 10.1002/fld

REFERENCES

1. Wagner C, Hüttl T, Sagaut P. *Large-Eddy Simulation for Acoustics*. Cambridge University Press: Cambridge, MA, 2006.
2. Terracol M, Manoha E, Herrero C, Labourasse E, Redonnet S, Sagaut P. Hybrid methods for airframe noise numerical prediction. *Theoretical and Computational Fluid Dynamics* 2005; **19**:197–227.
3. Tam CKW, Webb JC. Dispersion-relation preserving finite difference schemes for computational acoustics. *Journal of Computational Physics* 1993; **107**:262–281.
4. Tam CKW. Computational aeroacoustics: issues and methods. *AIAA Journal* 1995; **33**(10):1788–1796.
5. Lele SK. Compact finite difference schemes with spectral-like resolution. *Journal of Computational Physics* 1992; **103**:16–42.
6. Sengupta TK, Sircar SK, Dipankar A. High accuracy schemes for DNS and acoustics. *Journal of Scientific Computing* 2006; **26**:151–194.
7. Sengupta TK, Jain R, Dipankar A. A new flux-vector splitting compact finite volume scheme. *Journal of Computational Physics* 2005; **207**:261–281.
8. Karniadakis G, Sherwin SJ. *Spectral/HP Element Method for Computational Fluid Dynamics*. Oxford Science Publications: Oxford, U.K.
9. Cockburn B, Karniadakis GE, Shu CW. *Discontinuous Galerkin Methods*: *Theory*, *Computation and Applications*. Springer: Berlin.
10. Burbeau A, Sagaut P, Bruneau CH. An improved limiter for higher-order RKDG methods. *Journal of Computational Physics* 2001; **169**:115–150.
11. Burbeau A, Sagaut P. Simulation of a viscous compressible flow pas a circular cylinder with high-order discontinuous Galerkin methods. *Computers and Fluids* 2002; **31**(8):867–889.
12. Ekaterinaris JA. High-order accurate, low numerical diffusion methods for aerodynamics. *Progress in Aerospace Sciences* 2005; **41**:192–300.
13. Sesterhenn J. A characteristic-type formulation of the Navier–Stokes equations for high order upwind schemes. *Computers and Fluids* 2001; **30**:37–67.
14. Vichnevetsky R, Bowles JB. *Fourier Analysis of Numerical Approximations of Hyperbolic Equations*. SIAM Studies in Applied Mathematics. SIAM: Philadelphia, PA.
15. Tam CKW, Auriault L. Time-domain impedance boundary conditions for computational aeroacoustics. *AIAA Journal* 1996; **34**(5):917–923.
16. Fung KY, Ju H, Tallapragada B. Impedance and its time-domain extensions. *AIAA Journal* 2000; **38**(1):30–38.
17. Fung KY, Ju H. Time-domain impedance boundary conditions with mean flow effects. *AIAA Journal* 2001; **39**(9):1683–1690.
18. Zhuang M, Chen RF. Applications of higher-order optimized upwind schemes for computational aeroacoustics. *AIAA Journal* 2002; **40**(3):443–449.
19. Shu CW, Osher S. Efficient implementation of essentially non-oscillatory shock capturing schemes II. *Journal of Computational Physics* 1989; **83**:32–78.
20. Kovasznay LSG. Turbulence in supersonic flow. *Journal of the Aeronautical Society* 1953; **20**(10):657–682.
21. Motsinger RE, Kraft RE. *Design and Performance of Duct Acoustic Performance*. Aeroacoustics of Flight Vehicles: Theory and Practice, Table 1, p. 184 (Chapter 14).

DOI: 10.1002/fld